INTERNATIONAL JOURNAL OF AUTOMOTIVE AND MECHANICAL ENGINEERING (IJAME)
ISSN: 2229-8649 e-ISSN: 2180-1606
VOL. 19, ISSUE 1, 9419 – 9432
DOI: https://doi.org/10.15282/ijame.19.1.2022.06.0725

ORIGINAL ARTICLE

Sensitivity Identification of Low-Frequency Cantilever Fibre Bragg Grating Accelerometer using Cascade-Forward Backpropagation Neural Network

N.S. Khalid[1,2], M.R. Rahim[1] and M.F. Hassan[1,*]

[1]College of Engineering, Universiti Malaysia Pahang, Kuantan, 26300 Pahang, Malaysia.
[2]DRB-HICOM University of Automotive Malaysia, Pekan, 26600 Pahang, Malaysia.

ABSTRACT – The frequency-dependent issues and instrumentation requirement for FBG sensors necessitate the identification of the sensitivity of the cantilever FBG accelerometer using machine learning. As result, this article presents a cascade-forward backpropagation (CFB) neural network with an orthogonally-phase chirp signal with a range of constant forcing frequency and steadily increasing base acceleration amplitude as its input. This input/output data set was numerically calculated by integrating modal model and Euler-Bernoulli beam approach (FBG-MM). The maximum amplitude of the base acceleration was 200 m/s^2 and the forcing frequencies and location of the FBG sensor mounted on the beam measured from the fixed end were 1 to 90 Hz and 0.03 m, respectively. The trained CFB predicted the wavelength shift very well, but it was restricted to one-half of the forcing frequencies of those used in the CFB training process, whereas the base acceleration is not an important element in determining the sensitivity of the FBG accelerometer. In terms of the FBG sensor's location on the beam, considering a few positions will greatly expand the CFB's capabilities. Future work will include the use of the trained CFB as "black-box sensitivity" for actual acceleration measurement, as well as the use of empirical data to replace the numerical FBG-MM as the input/output training data set.

ARTICLE HISTORY
Received: 2nd Aug 2021
Revised: 20th Jan 2022
Accepted: 25th Feb 2022

KEYWORDS
FBG accelerometer;
FBG-MM;
CFB neural network;
Sensitivity identification;
Frequency-dependent

INTRODUCTION

The superior characteristics of fibre Bragg gratings (FBG) as a transducer have increased interest among researchers and industrial players. FBG is capable of operating in hazardous environments, providing multiple sensing points on a single cable, remote sensing, and being impervious to electromagnetic fields. These advantages enable FBG to be used in a wide variety of measurement applications, including vibration monitoring in gas exploration, military vehicles, and footbridges [1-4]; pressure measurement in pipeline leakage detection [5]; temperature monitoring in lubricating oil; and aircraft engine control systems [6]. However, the main concern of FBG in acceleration measurement is sensitivity, which is directly related to the reliability of the accelerometer. Teven et al. [7] addressed the sensitivity of the FBG accelerometer early on, using a simple harmonic oscillator to generate less than 1ug. Kersey et al. [8] demonstrated that the Fabry–Pérot accelerometer has high sensitivity and linearity, but no sensitivity value is given. Gerges et al. [9] then adapted and integrated the Fabry-Perot principle with a diaphragm-type FBG accelerometer, resulting in increased sensitivity. Weng et al. [10] continued to study Gerges et al. successful's work but with the addition of a U-shape rigid cantilever beam that produced 100 pm/g; this novel mechanism was developed to increase the vibratory effect. Meanwhile, Muller et al. [11] presented a two-diaphragm FBG accelerometer with a reported sensitivity of 1 pm/g in order to minimise cross-coupling of non-directional accelerations. Liu et al. [12] also presented the concept of two diaphragms with a distinct design, with a reported sensitivity of 45.9 pm/g.

Researchers have proposed various design and encapsulation techniques to improve the sensitivity of the FBG accelerometer. The introduction of a tip mass is one of the most well-known methods in cantilever beam FBG accelerometer [1, 13-18] Gagliardi et al. [1] presented the use of a tip mass in conjunction with laser-based interrogation methods to increase sensitivity and frequency response range, but no sensitivity value was provided. Basumallick et al. [13, 14] also considered the addition of tip mass, where the sensitivity found at 450 pm/g was improved by tailoring the effective distance between the sensor axis and the neutral axis of the cantilever. In their most recent work [18], the sensitivity can be increased to 450 pm/g by introducing a patch element between the FBG sensor and the beam. On the other hand, elastic diaphragm FBG accelerometers were discovered to have high sensitivity and resonant frequency, and are commonly available with single [19] or double diaphragms [11, 12, 20, 21]. Furthermore, Liu et al. [12, 21] demonstrated that double-point encapsulation improves FBG accelerometer sensitivity. Moreover, double-point encapsulation can effectively prevent FBG chirp, spectrum split, and wavelength detection ineffectiveness. A combination of cantilever beam and single diaphragm was also proposed, with extremely high sensitivity for approximately 100 pm/g [10].

The process of determining the sensitivitiy of the FBG accelerometer can be accomplished in two methods: (i) through prediction of the sensitivity using numerical data computed from the FBG accelerometer's mathematical model; or (ii)

*CORRESPONDING AUTHOR | M. F. Hassan | ✉ firdaus@ump.edu.my

through identification of the sensitivity using empirical data obtained from real acceleration measurements. Li et al. [22] proposed an ultra-compact FBG accelerometer and determined its sensitivity to be 244 pm/g and 633 pm/g using numerical and empirical data, respectively. Both numerical and empirical data are generated with a forcing frequency of 5 Hz and a steadily increasing base acceleration. In contrast to Li et al. [22], Liu et al. [23] calculated the sensitivity of the symmetrical bent spring plates FBG accelerometer using: (i) numerical data at a single maximum base acceleration of 1 m/s^2 at two forcing frequencies of 5 and 10 Hz, and (ii) empirical data at maximum base accelerations between 1 and 6 m/s^2 and forcing frequencies of 5, 10, 15, and 20 Hz (see Figure 1). The sensitivity was determined to be 1067 pm/g using numerical data, which is comparable to the empirical value found. Despite this, the sensitivity of the FBG accelerometer increases slightly with increasing forcing frequencies (1067 pm/g at 5 Hz, 1084 pm/g at 10 Hz, 1126 pm/g at 15 Hz, and 1166 pm/g at 20 Hz).

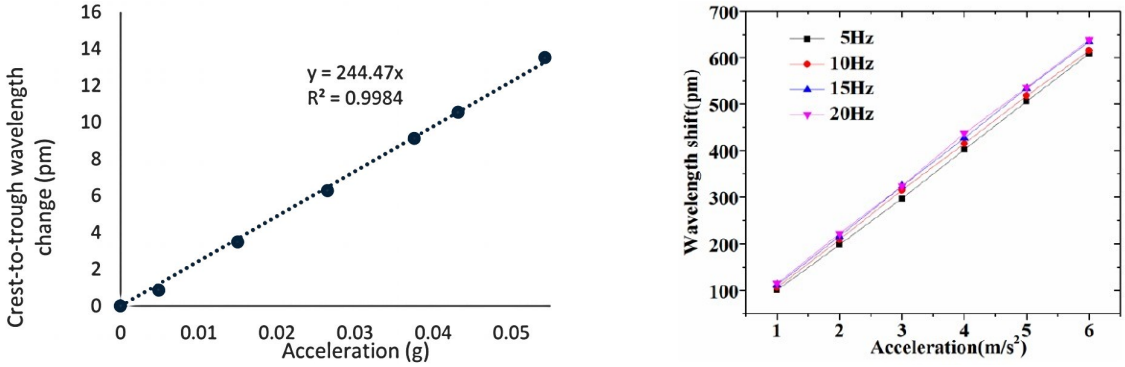

(a) (b)

Figure 1. Wavelength shift of the FBG accelerometer: (a) under different base acceleration at single forcing frequency of 5 Hz [22]; and (b) under different base accelerations and frequencies [23].

Based on the results of [23], it is possible to conclude that the wavelength shift of the FBG accelerometer is essentially frequency-dependent. In contrast to most common analogue voltage/electrical-charge accelerometers, the sensitivity is relatively flat over a wide frequency range, as illustrated in Figure 2, cited from one of the well-known vibration tool manufacturers [24]. Even though the sensitivity of the FBG accelerometer in [22] is linear, the sensitivity is computed at a single forcing frequency of 5 Hz rather than against a wide range of frequencies as in [24]. As proposed by the authors in [25], the cantilever FBG accelerometer was modelled using the more accurate approach, namely FBG-MM. Using this FBG-MM, it is discovered that the predicted amount of wavelength shift is frequency-dependent, and the sensitivity has yet to be discussed. As compared to [23], the relationship between wavelength shift and base acceleration was non-linear, and its sensitivity could not be fit using any basic fitting method, such as polynomial, etc.

To address the frequency-dependent issue, the authors have proposed in the primary study to use a cascade-forward backpropagation neural network to identify the sensitivity of a cantilever FBG accelerometer [26]. This identification process uses two input data to the network which is the maximum base acceleration and forcing frequency range from 0 to 90 Hz comes from sinusoidal signal and wavelength shift as its output. Unfortunately, in real application of the FBG accelerometer, the forcing frequencies are unknown beforehand, thus prescribing the forcing frequencies, as its input is deemed an inappropriate technique. As a result, this paper proposes a cascade-forward backpropagation neural network to identify the sensitivity of a cantilever FBG accelerometer using a single input, a chirp acceleration with a range of 0 to 200 m/s^2 and a forcing frequency of 0 to 90 Hz.

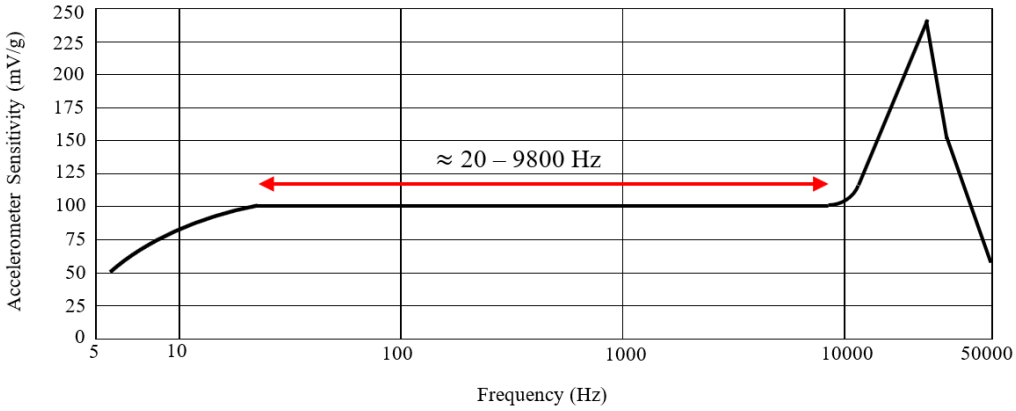

Figure 2. Accelerometer sensitivity (mV/g) for analogue voltage/electrical-charge accelerometer [24].

Data Extraction from Numerical and Empirical Data for Sensitivity Identification

Sensitivity is typically expressed in units of mV/g for an analogue-voltage based accelerometer. This sensitivity, which is documented in a calibration certificate, must come together with the accelerometer's datasheet. The use of an analogue-voltage accelerometer with vibration data acquisition and software does not necessitate a complicated setup; it is most likely a plug-and-play instrument. However, in the case of the FBG sensor, where the measurement is wavelength shift, the acceleration given to the FBG accelerometer may not be as simple to translate as in the case of the voltage-based accelerometer. Some kind of investigation into the relationship between the given acceleration and wavelength shift must be carried out, using either numerical or empirical data. Figure 3 demonstrates the procedure for obtaining these data as follows:

a) Identification of sensitivity using empirical data obtained from an actual FBG accelerometer
   i. The actual FBG accelerometer is mounted on a shaker;
   ii. A set of acceleration inputs must be provided to the shaker, which must be initialised by the voltage and signal profile from the measurement software (DASYLab);
   iii. The optical spectrum analyser's software is used to record the wavelength shift output from the FBG accelerometer (SENSE); and
   iv. These acceleration inputs in a(ii) and wavelength shift outputs in a(iii) are then used to computed the sensitivity.

b) Identification of sensitivity using the FBG accelerometer's numerical model
   i. The set of acceleration can be taken as either (i) the set of acceleration input as used in a(i) or (ii) prescribed acceleration;
   ii. This set acceleration is fed into the FBG-MM in order to obtain the wavelength shift output; and
   iii. These acceleration inputs in b(i) and wavelength shift outputs in b(ii) are then used to calculate the sensitivity.

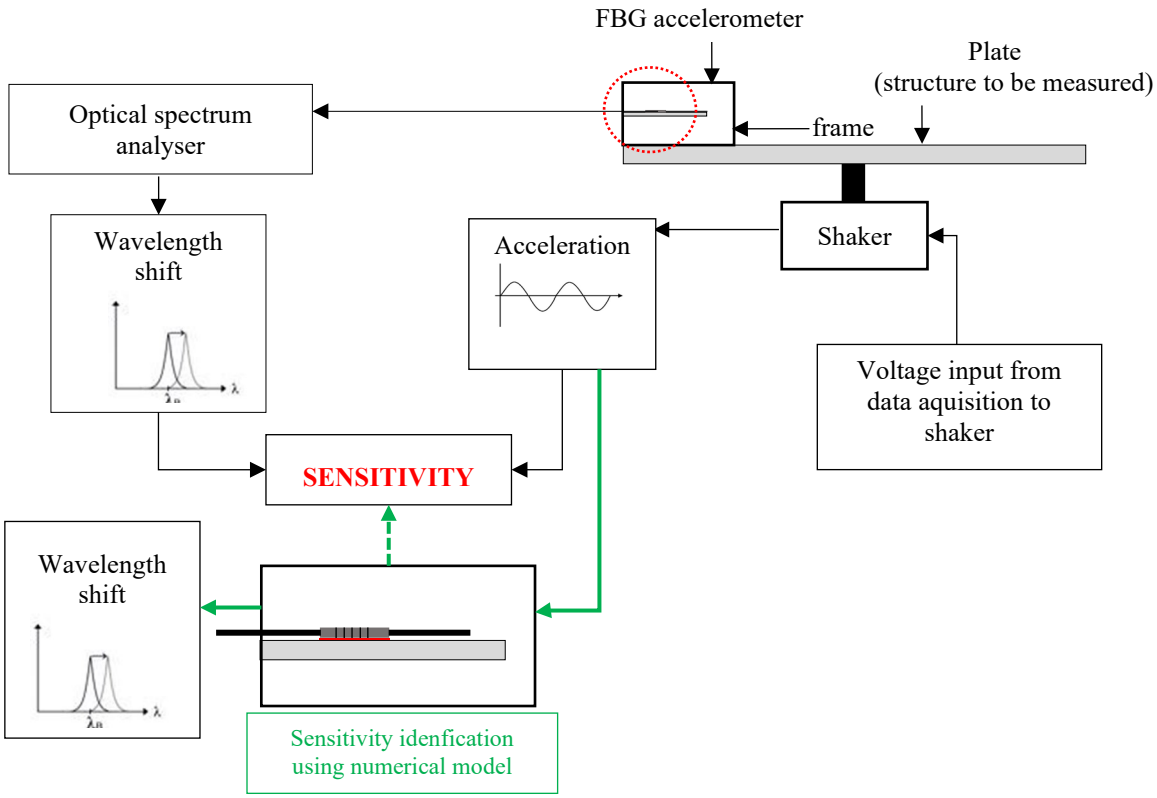

Figure 3. Measurement set-up for FBG accelerometer for real acceleration measurement and/or sensitivity identification.

BASIS FOR NON-PARAMETRIC IDENTIFICATION OF SENSITIVITY OF THE FBG ACCELEROMETER

Figure 4 depicts the measurement configuration of a cantilever FBG accelerometer, as well as its absolute motion due to base motion. The base excitation of the FBG accelerometer resulted in the strain being computed based on the relativity between the absolute motion and the base motion. Previous publication [25] provides a detailed derivation for the relative motion of a cantilever FBG accelerometer.

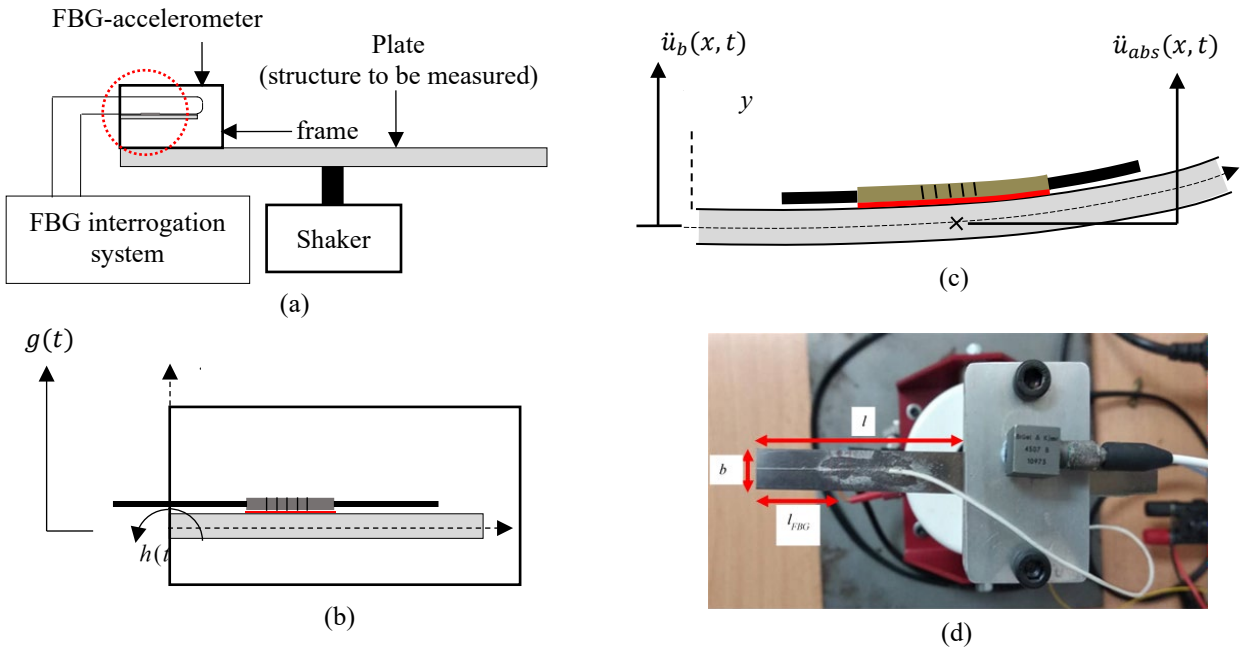

Figure 4. (a) Cantilever FBG accelerometer measurement configuration; (b) close-up of cantilevered FBG accelerometer (red dotted circle) under translational and rotational base motions; (c) absolute motion of FBG due to shaker-accelerated base motion; and (d) actual cantilever FBG accelerometer.

The mathematical model of the cantilever FBG accelerometer resulting from the application of the Euler–Bernoulli theorem and the modal model approach, namely, FBG-MM, can be used to construct the basis for identification [25]. Under base excitation, the steady-state response of the cantilevered FBG accelerometer is given as:

$$u_{rel}(x,t) = 2U_0 e^{i\omega t} \sum_{r=1}^{\infty} \left(\left[cosh\frac{\lambda_r}{L}x - cos\frac{\lambda_r}{L}x - \sigma_r \left(sinh\frac{\lambda_r}{L}x - sin\frac{\lambda_r}{L}x \right) \right] \frac{\sigma_r}{\lambda_r} \frac{\omega^2}{\omega_r^2 - \omega^2} \right) \tag{1}$$

where, $U_0 e^{i\omega t}$, σ_r, ω_r, ω, λ_r are harmonic base displacement, a constant for mode 'r', natural frequency of mode 'r', the forcing frequency, and the dimensionless frequency numbers, in that order. Equation (1) is used to calculate the beam curvature in Eq. (3), which reflects the amount of strain and wavelength shift of the FBG sensor; the strain of the FBG sensor is given as:

$$\varepsilon_{FBG}(x,t) = -(h + h_f) \frac{\partial^2 u_{rel}(x,t)}{\partial x^2} \tag{2}$$

where,

$$\frac{\partial^2 u_{rel}(x,t)}{dx^2} = 2U_0 e^{i\omega t} \sum_{r=1}^{\infty} \left(\frac{\lambda_r}{L} \right)^2 \left(\left[cosh\frac{\lambda_r}{L}x + cos\frac{\lambda_r}{L}x - \sigma_r \left(sinh\frac{\lambda_r}{L}x + sin\frac{\lambda_r}{L}x \right) \right] \frac{\sigma_r}{\lambda_r} \frac{\omega^2}{\omega_r^2 - \omega^2} \right) \tag{3}$$

The wavelength shift of the FBG is known to be directly proportional to the strain of the FBG, as shown in Eq. (4) [14, 18].

$$\Delta\lambda \approx 1.2 \times \varepsilon_{FBG}(x,t) \tag{4}$$

where, 1.2 denotes FBG strain sensitivity with peak wavelengths in the C band regime (1.2 pm/ in general). In comparison to the SDOF model proposed by [27], the FBG strain is given as:

$$\varepsilon_{FBG} = \frac{6(L-x)m}{bd^2E} \ddot{u}_b(x,t) \tag{5}$$

The sensitivity of the FBG sensor is given as:

$$S = \frac{\Delta\lambda}{\ddot{u}_b(x,t)} \tag{6}$$

Replacing both the FBG-MM (in Eq. (2)) and the SDOF model (in Eq. (5)) into Eq. (6) resulted in the sensitivity of the FBG accelerometer, as shown by Eqs. (7) and (8).

$$S_{FBG-MM} = \frac{1.2 \times \varepsilon_{FBG}}{\ddot{u}_b(x,t)} \tag{7}$$

$$S_{SDOF} = \frac{7.2(L-x)m}{bd^2E} \tag{8}$$

It is evident that the sensitivity computed by the FBG-MM model (in Eq. (7)) is affected by the position of the FBG sensor (x), time (t), and forcing frequency (ω). Meanwhile, the SDOF model (in Eq. (8)) is only dependent on the position of the FBG sensor (x) and is no longer affected by time (t) and forcing frequency (ω). Figure 5(a) and 5(b) show plots of wavelength shift versus base acceleration for the FBG-MM and SDOF models, respectively. The wavelength shift increases linearly as the base acceleration increases in the SDOF model (Figure 5(b)), unaffected by the varying forcing frequencies. Nevertheless, the wavelength shift computed by FBG-MM (Figure 5(a)) was significantly affected by the forcing frequencies, making it difficult to determine its sensitivity.

The sensitivity of the FBG accelerometer SDOF model can be easily determined using a simple polynomial function, but in the case of the FBG-MM, the polynomial function may result in inconsistency in the predicted wavelength shift. As a result, using artificial intelligence, such as genetic algorithms (GA) and fuzzy logic, among others, is one of the best candidates for determining its sensitivity. The authors prefer to propose neural network identification in this paper because it has been used successfully by the co-author of this work in identifying the foil-air bearing forces [28].

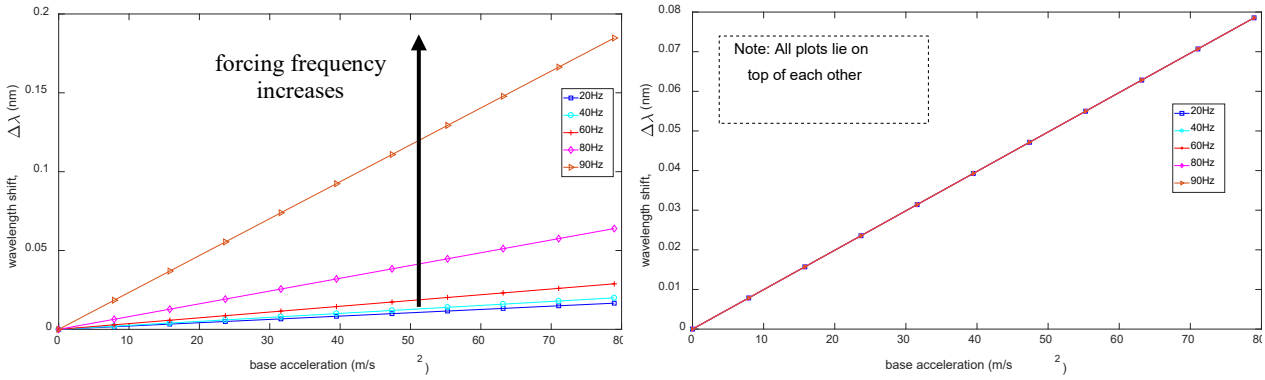

Figure 5. The wavelength shift plot against base acceleration for (a) FBG-MM; and (b) SDOF model.

NEURAL NETWORK IDENTIFICATION

In this research, a non-parametric model called a cascade-forward backpropagation neural network (CFB) is proposed, in which inputs from previous layers are fed to subsequent layers [29]. Figure 6 depicts the schematic diagram of the network and the scheme used to train it. The chirp base acceleration, $\ddot{u}_b(x,t)$ over a range of forcing frequency, ω will be the CFB's inputs. These inputs are normalised to a range of [–1, 1] [29] before being fed into the network (where $\widetilde{\ddot{u}_b}(x,t)$, $\widetilde{\Delta\lambda}$ and $\widetilde{\Delta\tilde{\lambda}}$ denote the network-normalised of the variable $\ddot{u}_b(x,t)$, $\Delta\lambda$ and $\Delta\tilde{\lambda}$, respectively). The network's output and its normalised form for the estimated $\Delta\lambda$ is denoted by $\Delta\tilde{\lambda}$ and $\widetilde{\Delta\tilde{\lambda}}$, respectively. In addition, Figure 6 depicts the identification (training) procedure, where the parameters of given assumed network architecture are optimised to minimise the difference (error) δ between the true (target) output $\Delta\tilde{\lambda}$ and the network output $\widetilde{\Delta\tilde{\lambda}}$, which is less than the specific convergence limit/tolerance.

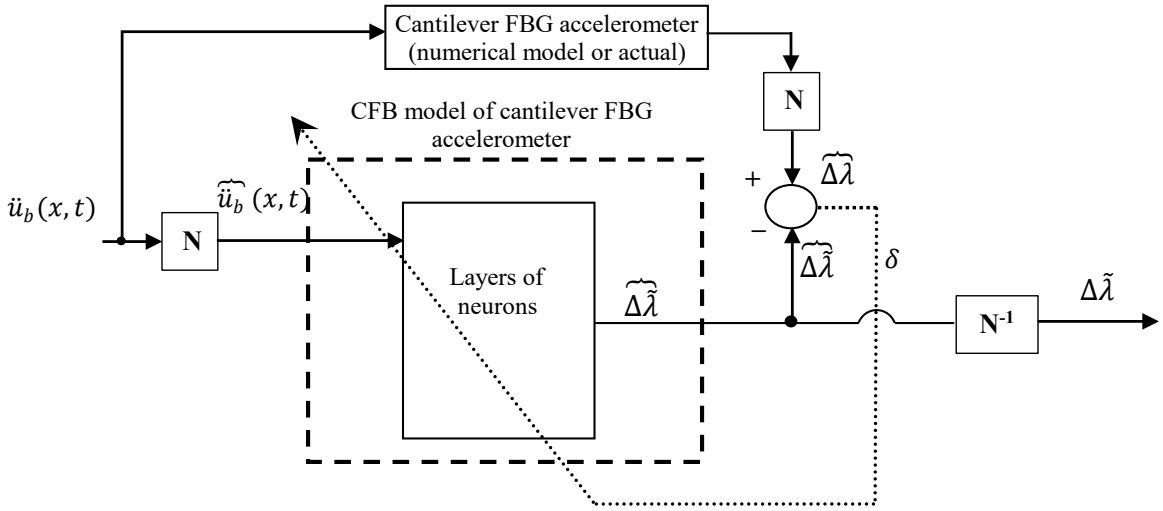

Figure 6. CFB model of the wavelength shift Δλ and its identification procedure (**N:** network normalisation; $\mathbf{N^{-1}}$**:** denormalisation).

Training Data Generation and Training Process

According to the FBG-MM theory and Figure 3 and Figure 4, identifying the sensitivity of an FBG accelerometer using CFB requires training data sets that include the true output for the given inputs. These data sets can be generated in two ways, depending on whether the identified cantilever FBG accelerometer is numerical or an actual transducer, as detailed in the Data Extraction from Numerical and Empirical Data for Sensitivity Identification subsection.

It is best practice to specify the harmonic base displacement $U_0 e^{i\omega t}$ as a sinusoidal form for an acceleration that consists of a single forcing frequency ω. These inputs, which are then replaced by $U_0 \sin \omega t$, are then substituted into Eq. (3), which provides the curvature of the beam. The wavelength shift is calculated using Eq. 3, as well as the dual-differentiation of $U_0 \sin \omega t$, resulting in input/output data to the FBG accelerometer, which will then be used for CFB training. The authors perform this data generation process in the preliminary research, where forcing frequencies are also considered as the second input to the CFB network.

In this paper, however, the wavelength shift is represented by orthogonally-phased chirp signals with constant forcing frequency ω and steadily increasing acceleration amplitude, $\ddot{U}$:

$$\ddot{u}_b(x,t) = \left(\frac{\ddot{U}_{b_{max}} - \ddot{U}_{b_{min}}}{t_{max} - t_{min}} t + \ddot{U}_{b_{min}}\right) \sin \omega t \tag{9}$$

It is worth noting that prescribing the chirp acceleration will result in the dual-integration of Eq. (9), yielding Eq. (10).

$$u_b(x,t) = -\frac{2\ddot{U}_{b_{min}} - 2\ddot{U}_{b_{max}} + \omega\ddot{U}_{b_{min}} t + \omega\ddot{U}_{b_{min}} t_{min} - \omega\ddot{U}_{b_{max}} t - \omega\ddot{U}_{b_{min}} t_{max})}{\omega^3 (t_{min} - t_{max})} \sin \omega t \tag{10}$$

Finally, Eq. (10) is subtituted into Eq. (3) and Eq. (4) subsequently to obtain the wavelength shift.

$$\Delta\lambda = 1.2 \times (h + h_f) \left[\left(\frac{2\ddot{U}_{b_{min}} - 2\ddot{U}_{b_{max}} + \omega\ddot{U}_{b_{min}} t + \omega\ddot{U}_{b_{min}} t_{min} - \omega\ddot{U}_{b_{max}} t - \omega\ddot{U}_{b_{min}} t_{max})}{\omega^3 (t_{min} - t_{max})} \sin \omega t\right) \left(2\sum_{r=1}^{\infty}\left(\frac{\lambda_r}{L}\right)^2 \left(\left[cosh\frac{\lambda_r}{L}x + cos\frac{\lambda_r}{L}x - \sigma_r\left(sinh\frac{\lambda_r}{L}x + sin\frac{\lambda_r}{L}x\right)\right]\frac{\sigma_r}{\lambda_r}\frac{\omega^2}{\omega_r^2 - \omega^2}\right)\right)\right] \tag{11}$$

These input/output data (wavelength shift – Eq. (11) and chirp base acceleration – Eq. (9)) are then fed into CFB for training purposes. Table 1 and [25] can be used as a reference for the mechanical properties of the cantilever beam.

Figure 7 depicts the entire procedure for determining the sensitivity of the cantilever FBG accelerometer using the CFB network. Meanwhile, Table 2 shows that the procedure begins with the preparation of the input/output data set using the chirp signal. The CFB network is then trained with a random number of hidden layers and neurons until it meets the criteria specified in the CFB algorithm. If the criterion is not met, the training process is repeated until the CFB criteria are met. The trained CFB network is then validated with a new set of input/output data for an efficiency test. Because some of the new input/output data sets used for validation are generated with parameters that differ from those used in

training, it is expected that the trained CFB will not be as perfect as desired. If this occurs, the training process can be stopped and trained CFB is said to be satisfactory. The process of generating data for validation purposes is covered in the results and discussion section.

Table 1. Properties of cantilever beam and FBG sensor.

Parameter	Value
Length, l	50 mm
Width, b	10 mm
Thickness, d	0.3 mm
Location of centre of FBG measured from fixed end, l_{FBG}	30 mm
Density, ρ	8000 kg/m^3
Young's Modulus, E	193 GPa
Poisson's ratio, υ	0.29
Wavelength of FBG sensor	1544 nm

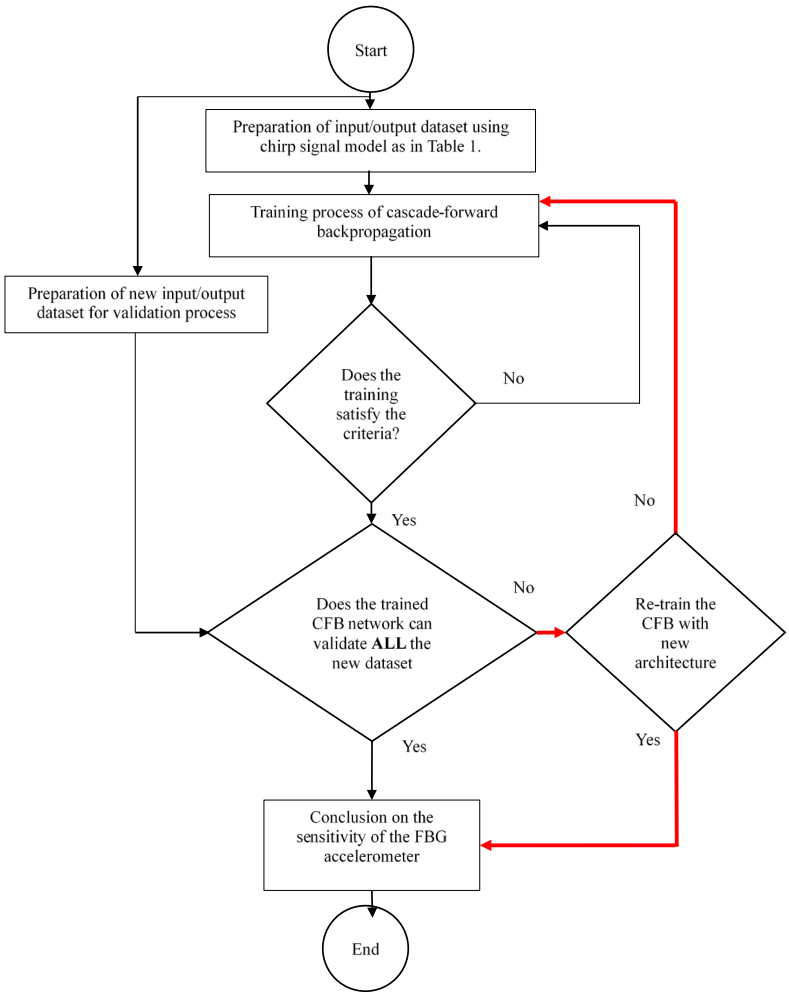

Figure 7. Complete process in the identification of sensitivity of the cantilever FBG accelerometer.

CFB Architecture and Training

Following several trial-and-error attempts, the best architecture for a CFB network was two hidden layers with 8 and 8 neurons, respectively (see Figure 8). The hidden and output layers used hyperbolic purelin and tangent sigmoid transfer functions, respectively, and the Levenberg–Marquardt optimisation method to optimise the weights and biases of network. The input/output data set is divided into 70% for training, 15% for validation, and 15% for testing. Meanwhile, $\mathbf{q}_k$ is defined as $1 \times k$ matrix that contains the input to layer no. 1.

$$\mathbf{q}_k = \left[\ddot{\boldsymbol{u}}_{\boldsymbol{b}_{f=1Hz}}\ \ddot{\boldsymbol{u}}_{\boldsymbol{b}_{f=2Hz}} \ldots \ddot{\boldsymbol{u}}_{\boldsymbol{b}_{f=90Hz}}\right] \tag{12}$$

where $\ddot{u}_b$ at each forcing frequency is a vector of input over a period of time t.

$$\ddot{\boldsymbol{u}}_{\boldsymbol{b}}(\boldsymbol{x}, \boldsymbol{t}_{(\boldsymbol{1}\rightarrow\boldsymbol{end})}) = \left[\ddot{u}_b(x, t_{(1)})\ \ddot{u}_b(x, t_{(2)}) \ldots \ddot{u}_b(x, t_{(end-1)})\ \ddot{u}_b(x, t_{(end)})\right] \tag{13}$$

The output of the *1st* layer as:

$$\mathbf{a}_k^{(1)} = \mathbf{h}^{(1)}\left(\boldsymbol{W}^{(1)}\boldsymbol{a}_k^{(1)} + \boldsymbol{b}^{(1)}\right) \tag{14}$$

While the output of the subsequent layer m^{th} layer are:

$$\mathbf{a}_k^{(m)} = \mathbf{h}^{(m)}\left(\boldsymbol{W}^{(m)}\boldsymbol{a}_k^{(m-1)} + \boldsymbol{W}^{(m)}\boldsymbol{a}_k^{(m-2)} + \boldsymbol{W}^{(m)}\boldsymbol{a}_k^{(m-3)} \ \ldots \ \boldsymbol{W}^{(m)}\mathbf{q}_k + \boldsymbol{b}^{(m)}\right), \quad m = 1, 2, \ldots M \tag{15}$$

where, $\mathbf{W}^{(m)}$ and $\mathbf{b}^{(m)}$ are the matrix of weights and vector of biases of the m^{th} layer, respectively; and $\mathbf{h}^{(m)}(\ \ )$ is a vector operator comprising the transfer functions of the neurons of the m^{th} layer.

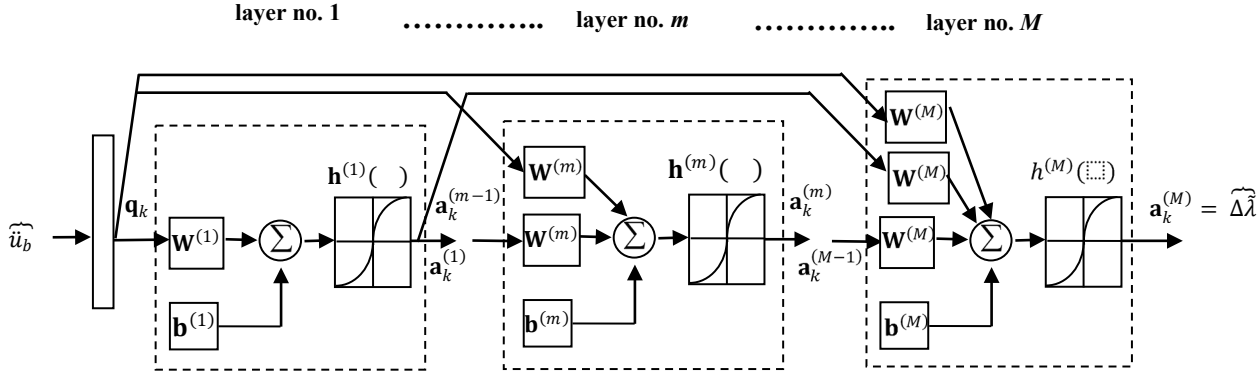

Figure 8. CFB model of the wavelength shift Δλ and its identification procedure.

Table 2 shows the input/output data set for the CFB training process. The left side of the table shows the chirp acceleration, while the right side shows the chirp wavelength shift computed from the FBG-MM model. The maximum and amplitude of the base acceleration are defined as $\ddot{U}_{b_{max}}$ and $\ddot{U}_{b_{min}}$, respectively with values of 200 and 1 m/s^2. There are 90 sets of input/output data that are combined in a single $1 \times k$ matrix (refer to Eqs. (12) and (14)) where k depends on the length of each data set and is 1,215,045 in this case. Only three sets of input/output at frequencies of 1, 2, and 90 Hz are presented to demonstrate how the amplitude chirp signal pattern looks. The forcing frequencies are limited to 90 Hz because the basic principle of the accelerometer allows it to operate at frequencies lower than its fundamental frequency (in this case, 95.6 Hz), thereby preventing the vibration signals from appearing much higher than they actually are [25].

RESULTS AND DISCUSSION

Along with the 15% of input/output data designated for validation during the CFB training process, a new set of input/output data was generated from FBG-MM for usage during the validation phase to examine the efficiency of the trained CFB's sensitivity. The following three input/output data sets are available:

i. Set 1 – input/output (base acceleration-wavelength shift) time series data with forcing frequencies ranging from 1 to 90 Hz and a maximum base acceleration of no more than 80 m/s^2 – within the range of the forcing frequencies and maximum base acceleration used in the training process (it means the maximum base acceleration does not exceed 200 m/s^2, the forcing frequency is less than 90 Hz and the position of the FBG sensor is 0.03 m from the fixed end of the cantilever beam);

ii. Set 2 – input/output (base acceleration-wavelength shift) time series data with forcing frequencies ranging from 1 to 90 Hz but with a maximum base acceleration greater than the maximum base acceleration used in the training process; and

iii. Set 3 – the forcing frequencies and maximum base acceleration of the time series of input-output (base acceleration-wavelength shift) data were randomly chosen, and the position of the FBG sensor on the cantilever beam was changed from 0.03 to 0.04 m.

An In-Depth Discussion of the Trained CFB Efficacy on Input/Output Data Set 1

As shown in Figure 9, the trained CFB accurately predicts the wavelength shift for input/output data set 1 at very low forcing frequencies of 10 and 15 Hz (Figure 9(a) and 9(b)). Increasing the forcing frequencies to 45 Hz results in an acceptable predicted wavelength shift where the maximum base acceleration is less than the actual wavelength shift computed by FBG-MM, as shown in Figures 9(c) and 9(d). It is worth mentioning that, as shown in Figures 9(e) and 9(f), if the forcing frequencies close to the maximum forcing frequency used in the CFB training process, the maximum base acceleration will decrease but the phase between the predicted and actual wavelength shift remains in phase. Despite the fact that all parameters in input/output data set 1 are within the range of those used in the CFB training process, the trained

CFB could not predict the wavelength shift very well as the forcing frequencies increased, especially when the forcing frequencies exceeded one-half of its fundamental frequency (45 Hz is around half of the 95.6 Hz). As a result, it can be concluded that the trained CFB can still be used to predict the wavelength shift of the FBG accelerometer, but the forcing frequencies must be less than or equal to 45 Hz. This limitation is acceptable because [23] once stated that the maximum forcing frequency of the FBG accelerometer should be approximately one-third or one-half of the fundamental frequency.

Table 2. Input and output data for CFB.

Input data	Ouput data
, $\ddot{u}_{b\,2\pi f} = \left(\frac{\ddot{U}_{b_{max}} - \ddot{U}_{b_{min}}}{t_{max} - t_{min}} t + \ddot{U}_{b\,min}\right) \sin(2\pi f t)$, Eq. 9	$\Delta\lambda = 1.2 \times \varepsilon_{FBG}(x,t)$, Eq. 11

$\ddot{U}_{b_{max}} = 200$ m/s^2 $\ddot{U}_{b_{min}} = 1$ m/s^2

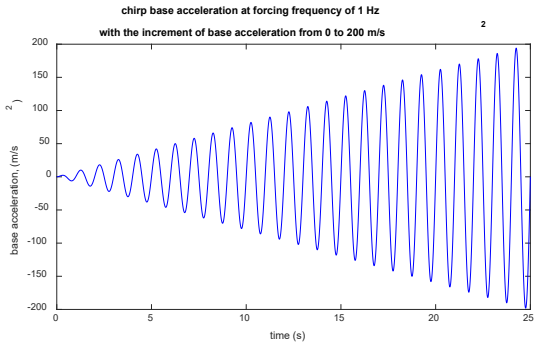

(a)

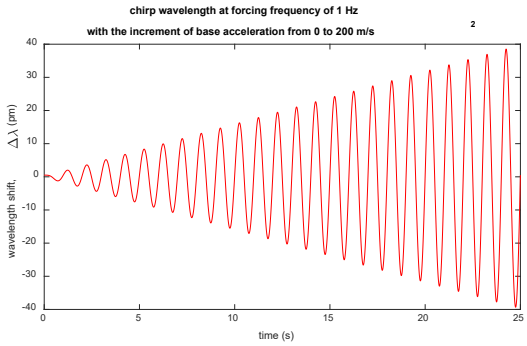

(b)

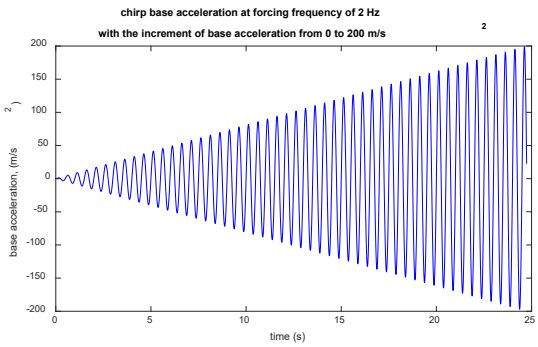

(c)

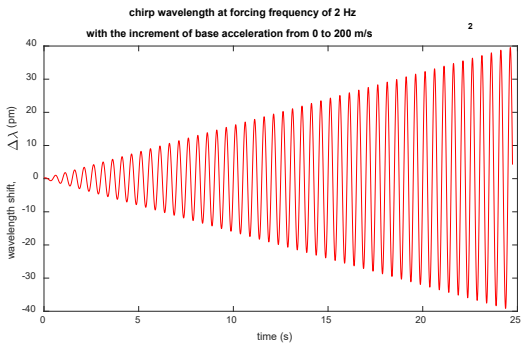

(d)

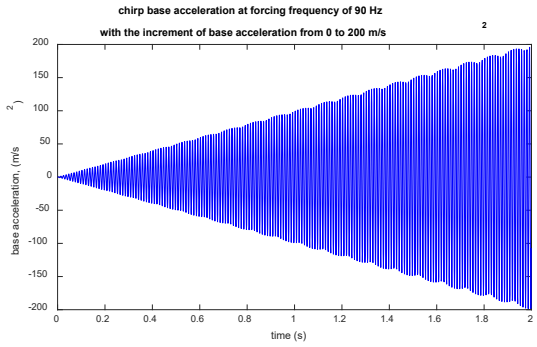

(e)

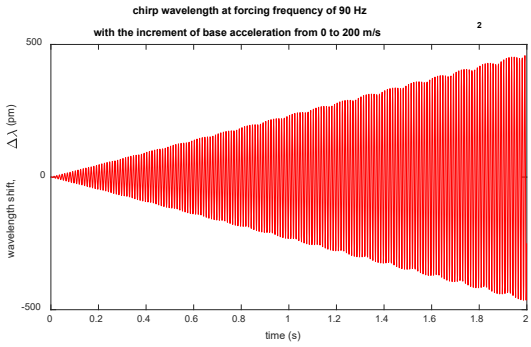

(f)

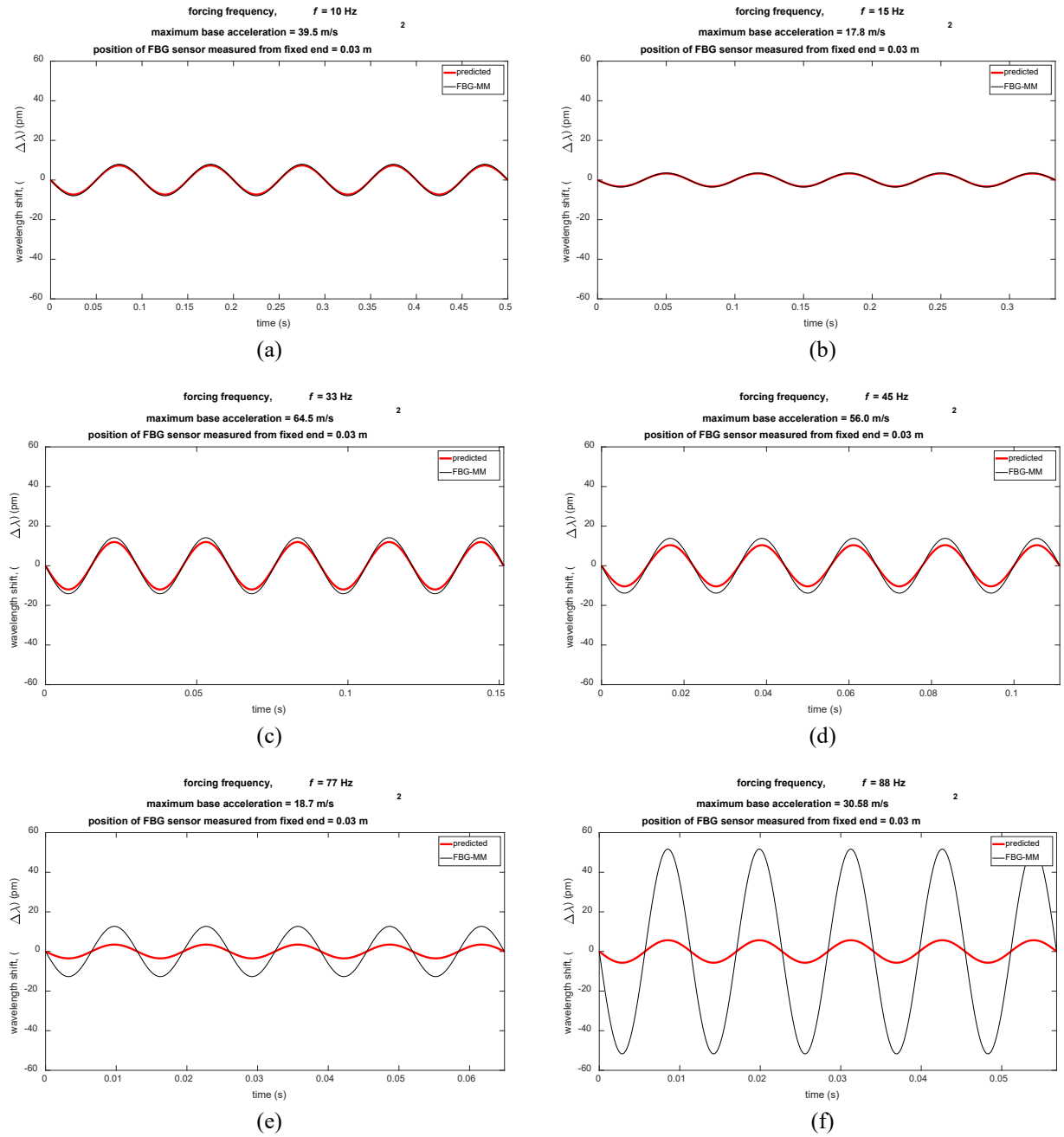

Figure 9. Predicted versus FBG-MM wavelength shift where the forcing frequencies, maximum base acceleration, and position of FBG sensor within the range of that used in the training process.

An In-Depth Discussion of the Trained CFB Efficacy on Input/Output Data Set 2

The input/output data set 2 data is used to investigate the CFB's ability to predict wavelength shifts when the maximum base acceleration is greater than the one used in the CFB training process. The frequencies of excitation used in this data set are similar to those used in set input/output data set 1. At forcing frequencies of 10, 15, 33, and 45 Hz and maximum base accelerations of 315.9, 266.5, 215.0, and 479.8 m/s^2, respectively (as in Figure 10(a) to 10(d)), the wavelength shifts exhibit a strong correlation with the actual wavelength shift computed by FBG-MM, with a slight decrement in its maximum base acceleration, similar to what was observed in the analysis of input/output data set 1. Notably, the prediction continues to remain acceptable for the extreme maximum base accelerations of 315.9 and 479.8 m/s^2, as in Figure 10(a) and 10(d). As was discovered previously when examining the efficacy of CFB using input/output data set 1, input/output data set 2 also demonstrates that as forcing frequencies to increase, the wavelength shift is underestimated without affecting its phase. Another observation is that, as illustrated in Figure 10(e) and 10(f), regardless of the magnitude of the maximum base acceleration (i.e., above the range of the CFB training process of greater than 200 m/s^2), the CFB could not accurately predict the wavelength shift when the forcing frequencies exceeded one-half of its fundamental frequency.

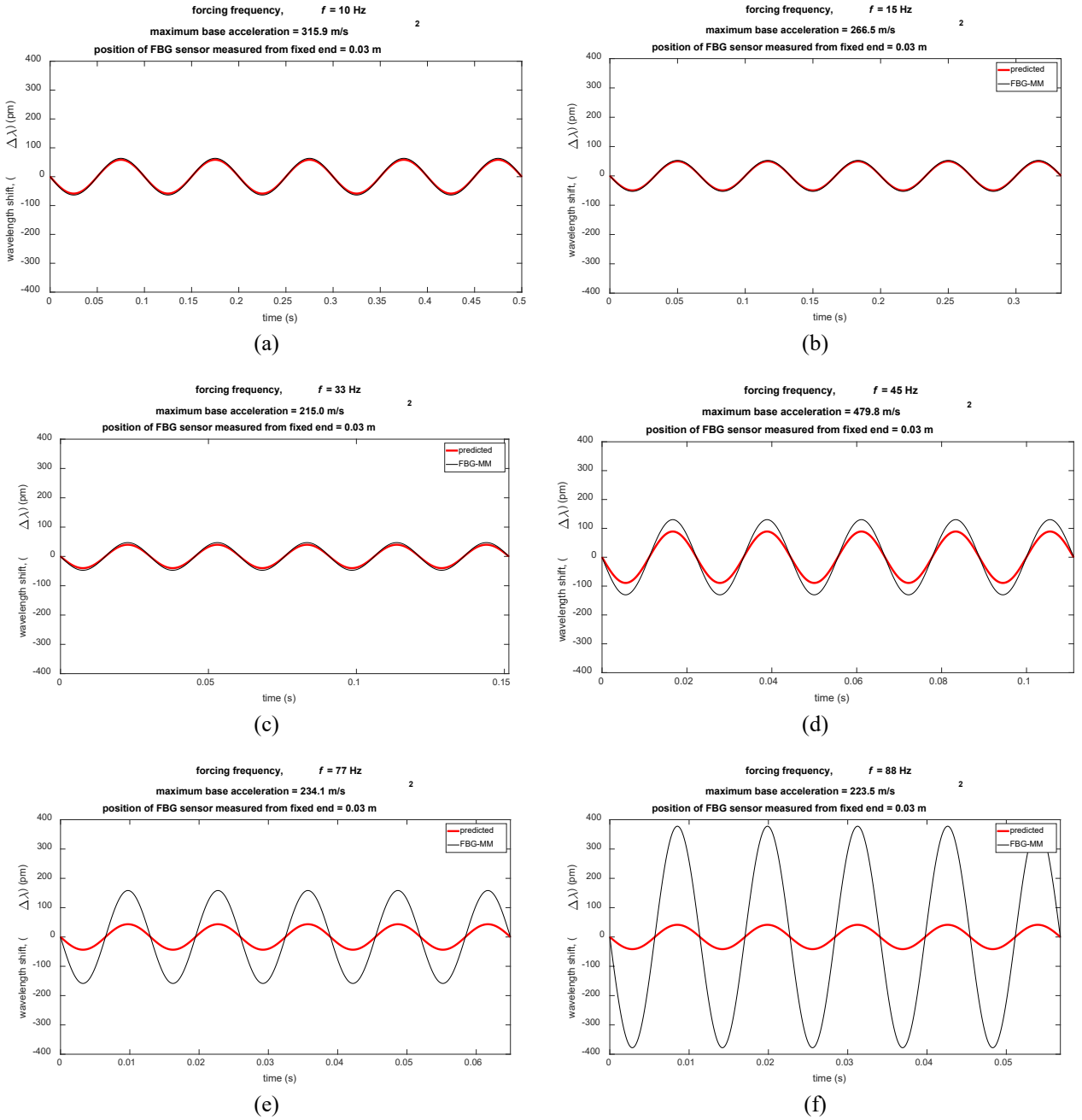

Figure 10. Predicted versus FBG-MM wavelength shift, where the forcing frequencies and position of FBG sensor within the range of that used in training process but with high maximum base acceleration.

An In-Depth Discussion of the Trained CFB Efficacy on Input/Output Data Set 3

The placement of the FBG sensor onto the beam also affects the sensitivity of the FBG accelerometer when developing a cantilever FBG accelerometer, as shown in Eq. (5). Refer to [25] for details on the effect of the placement of FBG sensor on the beam. In this subsection, the input/output data set is generated at random from the following combinations:

i. The forcing frequency and maximum base acceleration are within the range of those used in the CFB training process, but the FBG sensor is 0.04 m from the fixed end of the beam;

ii. The maximum base acceleration is within the range of those used in CFB training, but the forcing frequency is slightly outside of those used in the CFB training process, and the FBG sensor is 0.04 m from the fixed end of the beam; and

iii. The forcing frequency and maximum base acceleration are far outside the range of those used in the CFB training process, and the FBG sensor is 0.04 m from the fixed end of the beam.

It should be noted that all of the results in Figure 11(a) to 11(f) are based on the input/output data set when the FBG sensor is placed 0.04 m from the end of the beam. Figure 11(a) and 11(b) show contradictory findings when compared to previous analyses using input/output data sets 1 and 2, despite the fact that forcing frequencies and maximum base acceleration are within the range of those used in the CFB training process. The discrepancy was that the predicted

wavelength shift was greater than the actual wavelength shift computed by FBG-MM but remained in the same phase. When the forcing frequencies are slightly higher than those used in the CFB training process, the predictions are the opposite of what is shown in Figure 11(a) and 11(b). It is predicted that the amplitude of the wavelength shift will decrease, but the phase will be 180 degrees off, as shown in Figure 11(c) and 11(d). When the forcing frequency and maximum base acceleration are significantly greater than those used in the FBG training process (in Figure 11(e) and 11(f)), the predicted wavelength shift is unsatisfactory in terms of amplitude and phase, and even worse exhibits a different response profile as illustrated in Figure 11(f). As a conclusion to input/output data set 3, it can be confirmed that the trained CFB is inapplicable to any input/output data generated with a different FBG sensor position than that used during the CFB training process.

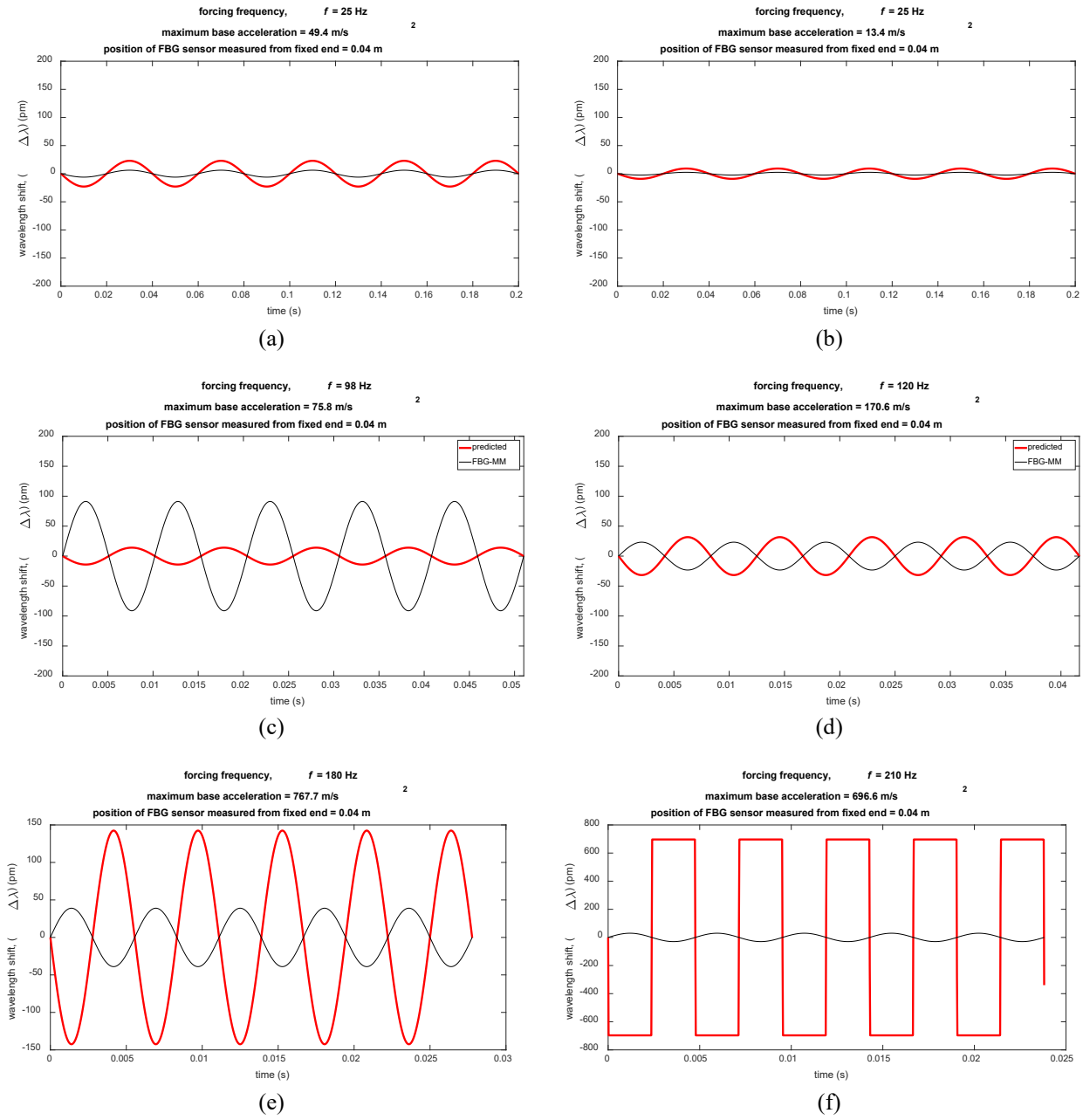

Figure 11. Predicted versus FBG-MM wavelength shift at random forcing frequencies maximum base acceleration but the position of the FBG changed to 0.04 measured from the fixed end.

CONCLUSION

This article discusses the process of determining the sensitivity of the FBG accelerometer using a cascade-forward backpropagation (CFB) neural network, by taking into account its frequency-dependent issues. It has been shown that the inclusion of the chirp signal is capable of overcoming the frequency-dependent problem in a CFB network when just a single input is fed in. The trained CFB predicted the wavelength shift remarkably well with forcing frequencies that are less than one-half of the fundamental frequency of the cantilever beam and, by coincidence, one-half of the forcing frequencies employed in the CFB training process. Furthermore, the trained CFB is unaffected by the amount of base

acceleration, suggesting that the amount of base acceleration is not the most significant factor in determining the sensitivity of the FBG accelerometer. The placement of the FBG sensor on the beam must also be varied in order to ensure that the input/output training data covers a broad variety of locations since a single position of the FBG sensor will not be able to enhance the CFB. Changes in the position of the FBG sensor, as previously mentioned, from its previous location to its new position (changed from 0.03 m to 0.04 m from the free end) resulted in an unacceptable prediction. In future works:

i. the trained CFB will be deployed in a real-acceleration experiment to determine the capabilities of a cantilever FBG accelerometer for predicting given accelerations;
ii. CFB network will be trained using an empirical input/output data set;
iii. the forcing frequencies employed in the CFB training process will be increased such that one-half of the permitted forcing frequencies will be two-thirds of the beam's fundamental frequencies;
iv. an orthogonally-phased chirp signal with steadily increasing forcing frequency ω and base acceleration amplitude $\ddot{U}$ will be introduced to generate a single input/output data set, in this way preventing numerous input/output data sets from being used; and
v. an additional mass at the cantilever tip may enhance the sensitivity of the FBG.

ACKNOWLEDGEMENT

The authors would like to thank the Ministry of Higher Education for providing financial support under Fundamental Research Grant Scheme (FRGS) No. FRGS/1/2019/TK03/UMP/02/29 (University reference RDU190191) and MyBrain15 programme, as well as Universiti Malaysia Pahang (www.ump.edu.my) for laboratory facilities.

REFERENCES

[1] G. Gagliardi *et al.*, "Design and test of a laser-based optical-fiber Bragg-grating accelerometer for seismic applications," *Meas. Sci. Technol.,* vol. 19, no. 8, p. 085306, 2008, doi: 10.1088/0957-0233/19/8/085306.
[2] Y. Zhang *et al.*, "Fiber Bragg grating sensors for seismic wave detection," in *Bruges, Belgium-Deadline Past*, 2005: International Society for Optics and Photonics, pp. 1008-1011.
[3] P. F. da Costa Antunes *et al.*, "Optical fiber accelerometer system for structural dynamic monitoring," *IEEE Sens. J.,* vol. 9, no. 11, pp. 1347-1354, 2009, doi: 10.1109/JSEN.2009.2026548.
[4] Y. Zhang, S. Li, Z. Yin, B. Chen, H.-L. Cui, and J. Ning, "Fiber-Bragg-grating-based seismic geophone for oil/gas prospecting," *Opt. Eng.,* vol. 45, no. 8, pp. 084404-084404-4, 2006, doi: 10.1117/1.2337631.
[5] J. Huang, Z. Zhou, D. Zhang, and Q. Wei, "A fiber Bragg grating pressure sensor and its application to pipeline leakage detection," *Adv. Mech. Eng.,* vol. 5, p. 590451, 2013, doi: 10.1155/2013/590451.
[6] H. A. Gebru and B. Padhy, "Fiber Bragg grating temperature sensor for defence and industrial applications," in *AIP Conf. Proc.*, 2011, vol. 1391, no. 1: AIP, pp. 434-436, doi: 10.1063/1.3643571.
[7] A. Tveten, A. Dandridge, C. Davis, and T. Giallorenzi, "Fibre optic accelerometer," *Electron. Lett.,* vol. 16, no. 22, pp. 854-856, 1980, doi: 10.1049/el:19800607.
[8] A. Kersey, D. Jackson, and M. Corke, "A simple fibre Fabry-Perot sensor," *Opt. Commun.,* vol. 45, no. 2, pp. 71-74, 1983.
[9] A. Gerges, T. Newson, J. D. Jones, and D. A. Jackson, "High-sensitivity fiber-optic accelerometer," *Opt. Lett.,* vol. 14, no. 4, pp. 251-253, 1989, doi: 10.1364/OL.14.000251.
[10] Y. Weng *et al.*, "A robust and compact fiber Bragg grating vibration sensor for seismic measurement," *IEEE Sensors J.,* vol. 12, no. 4, pp. 800-804, 2011.
[11] M. S. Muller, T. C. Buck, and A. W. Koch, "Fiber Bragg grating-based acceleration sensor," In Optomechatronic Technologies, 2009. ISOT 2009. International Symposium, 2009: IEEE, pp. 127-132, doi: 10.1109/ISOT.2009.5326111..
[12] Q. Liu, X. Qiao, H. Fu, H. Gao, and D. Yu, "Large frequency range and high sensitivity fiber Bragg grating accelerometer based on double diaphragms," *IEEE Sens. J.,* vol. 14, no. 5, pp. 1499-1504, 2014, doi: 10.1109/JSEN.2013.2296932.
[13] N. Basumallick *et al.*, "Fibre Bragg grating based accelerometer with extended bandwidth," *Meas. Sci. Technol.,* vol. 27, no. 3, p. 035008, 2016, doi: 10.1088/0957-0233/27/3/035008.
[14] N. Basumallick *et al.*, "Fiber Bragg grating accelerometer with enhanced sensitivity," *Sens. Actuator A Phys.,* vol. 173, no. 1, pp. 108-115, 2012, doi: 10.1016/j.sna.2011.10.026.
[15] W.-g. Zhang *et al.*, "Principles and realizations of FBG wavelength tuning with elastic beams," *Optoelectron. Lett.,* vol. 1, no. 1, pp. 5-9, 2005, doi: 10.1007/BF03033603.
[16] Y. Zhu *et al.*, "Fiber Bragg grating accelerometer with temperature insensitivity," *Microw. Opt. Technol. Lett.,* vol. 37, no. 2, pp. 151-153, 2003, doi: 10.1002/mop.10852.
[17] Y. Zhu *et al.*, "Temperature-insensitive fiber Bragg grating accelerometer," *IEEE Photon. Technol. Lett.,* vol. 15, no. 10, pp. 1437-1439, 2003, doi: 10.1109/LPT.2003.818048.
[18] N. Basumallick, P. Biswas, K. Dasgupta, and S. Bandyopadhyay, "Design optimization of fiber Bragg grating accelerometer for maximum sensitivity," *Sens. Actuator A Phys.,* vol. 194, pp. 31-39, 2013, doi: 10.1016/j.sna.2013.01.039.
[19] Q. P. Liu *et al.*, "Novel fiber Bragg grating accelerometer based on diaphragm," *IEEE Sens. J.,* vol. 12, no. 10, pp. 3000-3004, 2012, doi: 10.1109/JSEN.2012.2201464.
[20] X. Li *et al.*, "Study on low-frequency characteristic of double-diaphragm fiber Bragg grating geophone," *J. Optoelectron. Laser,* vol. 21, no. 4, pp. 529-532, 2010.
[21] Q. Liu *et al.*, "Design and modelling of a high sensitivity fiber Bragg grating-based accelerometer," *IEEE Sens. J.,* 2019. vol. 19, no. 14, pp. 5439-5445, doi: 10.1109/JSEN.2019.2904218.
[22] K. Li *et al.*, "Ultra-small fiber Bragg grating accelerometer," *Appl. Sci.,* vol. 9, no. 13, p. 2707, 2019, doi: 10.3390/app9132707.

[23] F. Liu, Y. Dai, J. M. Karanja, and M. Yang, "A low frequency FBG accelerometer with symmetrical bended spring plates," *Sensors,* vol. 17, no. 1, p. 206, 2017, doi: 10.3390/s17010206.
[24] N. Instruments. "Measuring Vibration with Accelerometers". [Online]. Available: https://www.ni.com/en-my/innovations/white-papers/06/measuring-vibration-with-accelerometers.html. [Accessed: May, 12 2021].
[25] N. S. Khalid, M. F. Hassan, M. H. Zohari, and M. R. Rahim, "A strain-wavelength modelling of low-frequency cantilever fibre Bragg grating accelerometer," *Proc. Inst. Mech. Eng. C: J. Mech. Eng. Sci.,* vol. 235, no. 35, p. 6711-6723, 2021, doi: 10.1177/09544062211008929.
[26] N. S. Khalid and M. F. Hassan, "Sensitivity identification of low-frequency cantilever fibre Bragg grating accelerometer," *Int. J. Integr. Eng.,* vol. 13, no. 7, pp. 235-244, 2021.
[27] T. T. Lam *et al.*, "Optical fiber three-axis accelerometer based on lasers locked to π phase-shifted Bragg gratings," *Meas. Sci. Technol.,* vol. 21, no. 9, p. 094010, 2010, doi: 10.1088/0957-0233/21/9/094010.
[28] M. F. B. Hassan and P. Bonello, "A neural network identification technique for a foil-air bearing under variable speed conditions and its application to unbalance response analysis," *J. Tribol.,* vol. 139, no. 2, 2017, doi: 10.1115/1.4033455.
[29] M. H. Beale, M. T. Hagan, and H. B. Demuth, "Neural network toolbox," *User's Guide, MathWorks,* vol. 2, pp. 77-81, 2010.